




Cite this: *J. Mater. Chem. A*, 2021, 9, 8480

Polyoxometalate-modified reduced graphene oxide foam as a monolith reactor for efficient flow catalysis of epoxide ring-opening reactions†

Xiaoting Jing, Zhen Li, Weijie Geng, Hongjin Lv, * Yingnan Chi * and Changwen Hu 

Continuous flow catalysis has been attracting significant interest due to its remarkable advantages over traditional batch reactions. In this work, a facile and broad-spectrum hydrothermal approach has been developed to construct polyoxometalate-modified reduced graphene oxide (POM@rGO) foam, which worked as a monolith reactor for efficient continuous flow catalysis of epoxide ring-opening reactions. The porous structures of rGO foam allow the high dispersion of the POM catalyst onto the substrate through electrostatic interactions. Specifically, a phosphotungstic acid ($\text{H}_3\text{PW}_{12}\text{O}_{40}$, denoted as PW_{12})-modified rGO (PW_{12} @rGO) monolith reactor exhibits remarkable catalytic activity and durability towards epoxide ring-opening reactions with alcohols, achieving 99% conversion and 92% selectivity for the methanolysis product in 10 min under ambient conditions without stirring. Notably, while coupling with a micro-injection pump, such PW_{12} @rGO foam can work as an efficient continuous flow reactor towards methanolysis of styrene oxide for 38 h with 99% conversion and over 90% selectivity, reaching a turnover number (TON) as high as 28 044.

Received 16th November 2020
Accepted 22nd February 2021

DOI: 10.1039/d0ta11188k

rsc.li/materials-a

Introduction

Continuous flow catalysis has received increasing attention as an ideal catalytic system for chemical synthesis in recent years.^{1–5} Compared to traditional batch reactions, continuous flow synthesis exhibits unique advantages of high efficiency, easy operation, and feasibility for scale-up production.^{6–8} Generally, in a flow reactor, the catalyst is immobilized onto a porous support. When the reaction solution flows through the reactor, a small amount of substrate can closely interact with an “excess” catalyst, thereby leading to an improved catalytic efficiency accordingly. Moreover, mechanical stirring and time-consuming separation steps (such as centrifugation and filtration) are not required in continuous flow catalysis and catalysts can be regenerated by simple rinsing with solvent. Monolith reactors,⁹ powder-packed reactors,¹⁰ and membrane-based reactors^{11,12} are three types of widely investigated flow reactors. However, the tight packing of powder catalysts in flow reactors often leads to the decrease of flow rate as well as the increase of column pressure. Although mixing powder catalysts with inert fillers can

reduce the column pressure, organic substrates cannot have effective access to the immobilized catalytic active sites. Therefore, the development of porous monolith-type flow reactors with high contact efficiency, favorable mass transfer, and excellent thermal stability is an interesting area to explore; the effective assembly of catalysts with monolithic materials remains still a substantial challenge for the fabrication of monolith-type flow reactors.

Polyoxometalates (POMs) represent a class of nano-sized metal-oxide polyoxoanion clusters, which are usually composed of corner- and edge-sharing $\{\text{MO}_x\}$ polyhedra ($\text{M} = \text{Mo}, \text{W}, \text{V}, \text{Nb}, \text{and Ta}$).^{13,14} Due to their structural diversity and tunable physicochemical properties (such as Brønsted acidity, the composition, reversible proton and electron storage, rich redox chemistry, *etc.*), POMs exhibit remarkable catalytic activity in a series of chemical transformations.^{15–17} Compared to traditional inorganic acids (*e.g.* H_2SO_4 , HNO_3 , and HCl), POMs, as one special type of solid polyacid, are much less corrosive and exhibit rich Brønsted acidity that can be precisely adjusted by varying their electronic structures and chemical compositions.¹⁸ Given the high adjustability and good solubility of POMs in various solvents, POM-based catalysts are often used in homogeneous catalysis, facing the difficulty of recyclability or reusability.¹⁹ To solve this problem and meet the concept of green chemistry, a number of heterogenized POM catalysts have been synthesized through immobilization onto suitable supports including carbons,^{18,20} zirconia,²¹ silica,²² MCM-41,²³ and metal-organic frameworks.^{24–26} Although these supported-

Key Laboratory of Cluster Science Ministry of Education, Beijing Key Laboratory of Photoelectronic/Electrochromic Conversion Materials, School of Chemistry and Chemical Engineering, Beijing Institute of Technology, Beijing, 102488, P. R. China. E-mail: chiyingnan7887@bit.edu.cn; hlv@bit.edu.cn

† Electronic supplementary information (ESI) available. See DOI: 10.1039/d0ta11188k

POMs have been widely used in catalyzing organic reactions, most of them are used as heterogeneous powder catalysts in traditional batch reactions. In contrast, few examples have been reported in constructing POM-containing flow reactors for chemical synthesis. For example, phosphotungstic acid was immobilized on hierarchically porous silica with the help of a pyrogallol layer and such monolithic catalysts used as flow reactors can promote the esterification reaction.²⁷ The mixture of polymer immobilized POM ionic liquids and silica was used to catalyze the oxidation of sulfides under continuous flow conditions.²⁸ However, the major concerns of the above-mentioned two examples are the leaching of POM catalysts during the reaction due to the weak interaction between the silica supports and POM catalysts, resulting in a decrease of catalytic performance with prolonged reaction time. Therefore, the development of appropriate porous supports to fabricate robust and efficient POM-based monolith flow reactors is of scientific significance.

As an interesting two-dimensional (2D) material, graphene-derived composites have been extensively studied especially in the fields of functional devices, chemical and biological sensors, and energy-storage materials.^{29–34} In addition, given its high surface area, good thermal/chemical stability and attractive adjustability, graphene has also been reported as a suitable support to immobilize POM catalysts.^{35–37} Recently, our group reported the construction of a compressible monolithic POM@GF reactor through the assembly of POM catalysts with elastic graphene foam, which exhibits high catalytic activity for biodiesel production.³⁸ Nevertheless, the approach used to construct such monolithic POM@GF catalysts was a bit complicated and time-consuming, which greatly prompts us to explore more facile and practical synthetic approaches for monolith reactor construction. Inspired by the pioneering work on the preparation of a three-dimensional (3D) graphene hydrogel from Shi's group,³⁹ the resulting 3D graphene hydrogel exhibits a well-defined and interconnected 3D porous network, good mechanical strength, and thermal stability, thereby working as a potentially excellent support to fabricate POM-based monolith reactors for continuous flow catalysis.

Herein, we report for the first time the construction of POM-containing monolithic reactors by assembling POM catalysts with 3D reduced graphene oxide (POM@rGO) foam under facile hydrothermal conditions. The resulting POM@rGO foam was systematically characterized using various techniques, revealing that the POM clusters are highly dispersed on surface of rGO foam through electrostatic interactions. Due to strong Brønsted acidity, a phosphotungstic acid ($\text{H}_3\text{PW}_{12}\text{O}_{40}$, denoted as PW_{12})-modified rGO (PW_{12} @rGO) monolith reactor exhibits remarkable catalytic activity and durability towards epoxide ring-opening reactions with alcohols, obtaining a 99% conversion of styrene oxide in 10 min at a selectivity of 92% for the methanolysis product. More importantly, such PW_{12} @rGO foam can work as an efficient continuous flow reactor towards methanolysis of styrene oxide for 38 h with 99% conversion and over 90% selectivity, reaching a turnover number (TON) as high as 28 044.

Experimental

Materials and methods

Styrene oxide (98%) was purchased from Meryer (Shanghai) Chemical Technology Co., Ltd. Pristine graphite powders (325 mesh), phosphotungstic acid (99%, PW_{12}), phosphomolybdic acid (98%, PMo_{12}) and silicotungstic acid (99%, SiW_{12}) were purchased from Shanghai Aladdin Biochemical Technology Co., Ltd. 2-Methoxy-2-phenylethanol (98%), 2-ethyloxirane (>99%), 2-methoxybutan-1-ol (97%), 2-(chloromethyl)oxirane (99%), 1-chloro-3-methoxypropan-2-ol (99%), 2-(butoxymethyl)oxirane (>98%), 2-phenyl-2-propoxyethanol (99%) and 1-butoxy-3-methoxypropan-2-ol (98%) were purchased from Shanghai Macklin Biochemical Co., Ltd. Biphenyl ($\geq 99\%$) and naphthalene (99%) was purchased from Alfa Aesar China (Tianjin) Co., Ltd. Hydrochloric acid (75%), potassium permanganate (99.5%), sulfuric acid (95–98%), sodium nitrate (99%), hydrogen peroxide (30 wt% in H_2O), methanol ($\geq 99.5\%$), ethanol ($\geq 99\%$), *n*-propanol (99%) and *i*-propanol ($\geq 99.7\%$) were supplied by Sinopharm Chemical Reagent Co., Ltd. All reagents and solvents were used as received without further purification.

The scanning electron microscope (SEM) images of the samples were obtained on a high-resolution scanning electron microscope FEI Quanta 400 FEG ESEM. Transmission electron microscope (TEM) images were recorded on an FEI Tecnai T12 with an acceleration voltage of 120 kV. Fourier transform infrared (FT-IR) spectra were recorded on a JASCO 6300D instrument by the KBr pellet method. X-ray powder diffraction (XRD) patterns were collected on a Bruker instrument (D8 Venture) using graphite-monochromatized $\text{Cu K}\alpha$ ($\lambda = 1.5406 \text{ \AA}$) radiation. The Raman spectra were recorded on an SNFT-SRLab1000 Raman microscope. The Brunauer–Emmett–Teller (BET) specific surface areas were measured using a Micrometrics ASAP 2000 instrument using nitrogen adsorption-desorption isotherms at 77 K. Pore size distributions were estimated using the Barrett–Joyner–Halenda (BJH) method. X-ray photoelectron spectroscopy (XPS) measurements were carried out on Thermo ESCALAB 250Xi with a monochromatized $\text{Al-K}\alpha$ X-ray source (1486.6 eV). UV-vis spectra were recorded on UV-2600. Inductively coupled plasma atomic emission spectrometry (ICP-AES) measurements were performed on a Thermo Scientific iCAPQ. The epoxide ring-opening reaction was monitored using a gas chromatograph (Shimadzu GC-2014C) equipped with a flame ionization detector (FID) and a HP-5 ms capillary column.

The acidity measurements of the samples

The acidic strength and acidity of the samples were tested by temperature programmed desorption of ammonia (NH_3 -TPD) using a PCA-1200. Initially, 11 mg of PW_{12} @rGO was dried at 150 °C for 30 min under an Ar flow. Then, at a flow rate of 30 mL min^{-1} , the sample was flushed with NH_3 at 80 °C for 30 min. After removing physically adsorbed NH_3 by flowing Ar at 80 °C for 30 min, the chemically adsorbed ammonia was determined by using a thermal conductivity detector (TCD) under the

condition of heating at $10\text{ }^{\circ}\text{C min}^{-1}$ up to $300\text{ }^{\circ}\text{C}$ and then it was kept for 60 min. The total acidity of the solid samples was further measured by the potentiometric titration method that could estimate the strength and the total number of acid sites of the solids.^{23,24} In typical measurements, the sample (0.1 g) was uniformly dispersed in 6 mL acetonitrile (Merck), and agitated for 2 h under ultrasonication. Subsequently, the suspension was titrated with 0.05 mol L^{-1} *n*-butylamine (Merck) in acetonitrile, which is added using a micro-injection pump at a rate of 0.05 mL min^{-1} . The electrode potential variation was measured with an OHAUS ST3100 digital PH meter under potential mode.

Synthesis of graphene oxide

Graphene oxide (GO) was prepared by oxidation of graphene powder (325 mesh) according to modified Hummers' method.³⁶ Generally, graphite (9.0 g) and sodium nitrate (4.5 g) were added into concentrated sulfuric acid (210 mL) under stirring and the solution was kept in an ice water bath for 2 h. Then, potassium permanganate (27 g) was slowly added and the temperature of the system was maintained at lower than $20\text{ }^{\circ}\text{C}$. After that, the mixture was transferred to a water bath of $35\text{--}40\text{ }^{\circ}\text{C}$ for 0.5 h, generating thick paste. Subsequently, 420 mL of deionized water was added. After stirring at $80\text{ }^{\circ}\text{C}$ for 20 min at $80\text{ }^{\circ}\text{C}$, additional 1000 mL of water was added. To complete the oxidation, 60 mL of H_2O_2 (30%) was slowly added to the above solution and the color of the solution turns from brown to yellow. The mixture was filtered to obtain a yellow precipitate which was further washed with deionized water, 1 : 1 HCl aqueous solution and 1 : 9 HCl aqueous solution, respectively, to remove the residual metal ions. The resulting solid was dispersed in water by sonication for 1 h to prepare a GO aqueous dispersion. The resulting brown dispersion was then centrifuged at 4000 rpm for 1 h and centrifuged at 10 000 rpm for another 1 h to remove any aggregates. Finally, GO was further purified by dialysis for a week.

The preparation of POM@rGO foam

10 mL of graphene oxide (GO) aqueous dispersion (2 mg mL^{-1}) and three kinds of POM $\text{H}_3\text{PW}_{12}\text{O}_{40}$ (PW_{12}), $\text{H}_3\text{SiW}_{12}\text{O}_{40}$ (SiW_{12}), and $\text{H}_3\text{PMo}_{12}\text{O}_{40}$ (PMo_{12}) (0.07 mmol) were mixed and sealed in a Teflon-lined autoclave, which was heated at $180\text{ }^{\circ}\text{C}$ for 12 h. After cooling to room temperature, the obtained POM@rGO block was taken out from the autoclave and then soaked in fresh distilled water for 3 days to remove any unsupported POM anions. The wet POM@rGO was transferred to a vessel and placed in liquid nitrogen. Then the vessel was placed in a freeze dryer for 3 days to obtain the dry sample of POM@rGO foam. The amount of PW_{12} loading was quantified using ICP-AES analyses. The experimental results reveal that 2.3 wt%, 3.6 wt%, and 4.7 wt% PW_{12} @GF monolith reactors (diameter: 10 mm, height: 10 mm, 20 mg) contain approximately 0.00016, 0.00025, and 0.00033 mmol PW_{12} species, respectively.

Epoxide ring-opening reactions catalyzed by the POM@rGO monolith reactor

A glass pipette (inner diameter: 5 mm) was used to make a glass column reactor by sealing its bottom part with a piece of cotton.

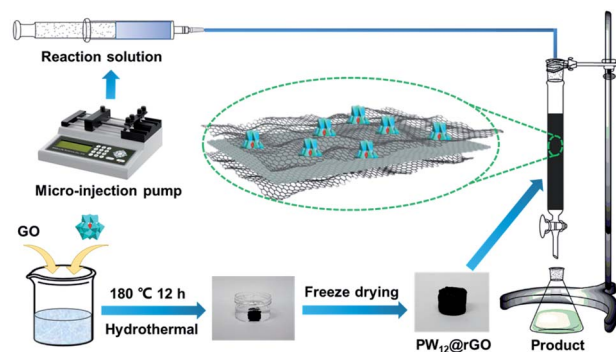
Such a glass column was packed with the small pieces of PW_{12} @rGO foam (0.25 g 4.7 wt%, corresponding to around 0.004 mmol PW_{12} active species). In a typical continuous flow catalysis, methanol solution containing styrene oxide (0.5 mmol mL^{-1}) and biphenyl (0.3 mmol mL^{-1}) was pumped into the packed glass column using a micro-injection pump (LSP02-1B) at a flow rate of 0.1 mL min^{-1} . The reaction solution passing through the reactor after catalysis was collected in separated vials as 1 mL aliquots and further analyzed and quantified by GC-FID at various time intervals.

Results and discussion

Synthesis and characterization of POM@rGO foam

Scheme 1 illustrates the general procedure of the construction of polyoxometalate-modified reduced graphene oxide (POM@rGO) foam using such a facile and broad-spectrum hydrothermal approach and subsequent continuous flow catalysis using the POM@rGO monolith reactor. This reported facile hydrothermal approach is applicable to fabricate POM@rGO foam using three Keggin-type POMs with different Brønsted acidities, PW_{12} , SiW_{12} , and PMo_{12} . The detailed experimental procedures were introduced in above Section 2.3; in the final step the wet sample was freeze-dried for three days to obtain the dry POM@rGO composites (Fig. S1†), which were further characterized by the powder XRD technique (Fig. S2†). The amount of loaded POM catalysts in the POM@rGO composite can be easily adjusted by changing the concentration of POM used in the hydrothermal reaction. As a representative example, the PW_{12} @rGO foam was systematically discussed in the following characterization.

The SEM image in Fig. 1c shows that GF has a well-defined and interconnected 3D porous network with a pore size of the network at the micro and sub-microscales, and the porous structures are formed through the stacking of graphene sheets (Fig. 1a). As shown in Fig. 1b, the sheet structure of graphene is maintained after the introduction of POMs, and the deposited POM clusters (the dark spots in Fig. 1b) are highly dispersed on the graphene sheets. In addition, the dispersion of POM on the graphene sheet layer is further confirmed by EDS and elemental



Scheme 1 Schematic illustration of the construction of POM@rGO foam and subsequent continuous flow catalysis using the POM@rGO monolith reactor.

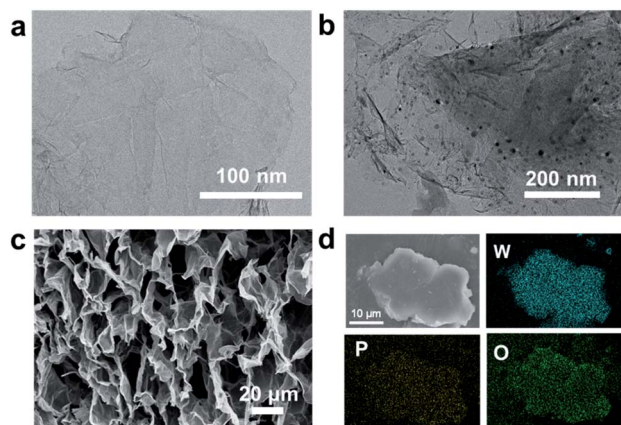


Fig. 1 (a) TEM image of rGO; (b) TEM images of $\text{PW}_{12}@r\text{GO}$; (c) SEM images of rGO; (d) EDS elemental mapping of the $\text{PW}_{12}@r\text{GO}$ monolith.

mapping measurements (Fig. 1d and S3[†]). The XRD patterns of PW_{12} , rGO, and $\text{PW}_{12}@r\text{GO}$ are shown in Fig. S2.[†] The characteristic diffraction peak of graphene oxide (GO) at $2\theta = 11.6^\circ$ completely disappeared in $\text{PW}_{12}@r\text{GO}$ revealing that GO is partially reduced under the hydrothermal conditions.³⁷ There are no diffraction peaks of Keggin-type PW_{12} crystals in the XRD pattern of $\text{PW}_{12}@r\text{GO}$, indicating that the polyanions are highly dispersed on the rGO support, which is consistent with the result of TEM measurements.

Fig. 2 shows the FT-IR spectra of PW_{12} , rGO, and $\text{PW}_{12}@r\text{GO}$. Three characteristic peaks at 1738 cm^{-1} (C=O), 1587 cm^{-1} (C=C) and 1246 cm^{-1} (C–O–C) belong to the characteristic absorption bands of rGO.³⁸ The Keggin-type PW_{12} cluster exhibits four characteristic peaks at 1077 cm^{-1} for P–O_a (a: central PO₄ tetrahedron oxygen atoms), 977 cm^{-1} for W=O_d (d: terminal oxygen atoms), 903 cm^{-1} for W–O_b–W (b: corner-shared oxygen atoms), and 789 cm^{-1} for W–O_c–W (c: edge-shared oxygen atoms), respectively.³⁹ The existence of POM characteristic absorption in the FT-IR spectrum of $\text{PW}_{12}@r\text{GO}$ further confirms the successful immobilization of PW_{12} . Notably, compared to the IR spectrum of the PW_{12} precursor, the vibration peak of W–O_c–W in $\text{PW}_{12}@r\text{GO}$ shows an obvious

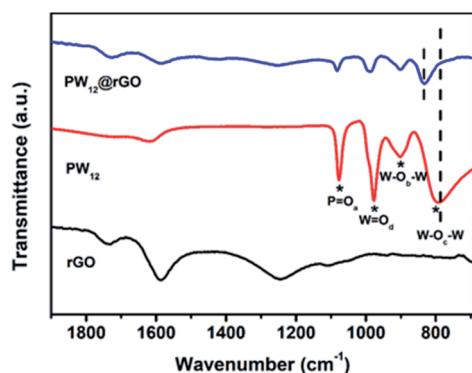


Fig. 2 FT-IR spectra of PW_{12} , rGO, and $\text{PW}_{12}@r\text{GO}$.

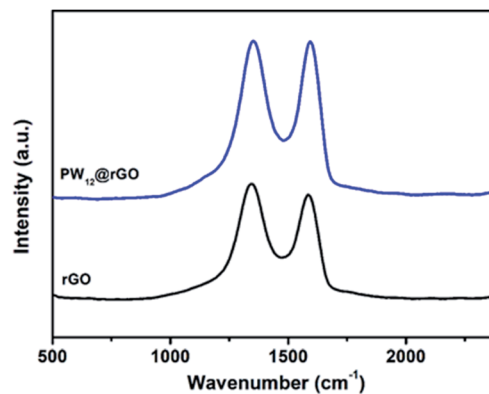


Fig. 3 Raman spectra of rGO and $\text{PW}_{12}@r\text{GO}$.

blue shift from 789 cm^{-1} to 832 cm^{-1} , indicating the strong interactions between PW_{12} and the rGO support. According to our previous investigation, the blue shift of the W–O_c–W vibration in the composite might be related to the electrostatic interaction through the protons located on O_c atoms.³⁵

Fig. 3 shows the characteristic vibrations of the D-band at 1345 cm^{-1} and the G-band at 1586 cm^{-1} in the Raman spectra of rGO and $\text{PW}_{12}@r\text{GO}$. The G-band signal is attributed to the planar sp^2 carbon and the D-band corresponds to the defects on graphene sheets.⁴⁰ Both the D/G band positions of $\text{PW}_{12}@r\text{GO}$ and the intensity ratio of the D and G bands (I_D/I_G) are similar to those of pristine rGO. The fact shows that the rGO structure is not greatly affected after the incorporation of POM. In addition, the N₂ adsorption–desorption isotherms of GF and $\text{PW}_{12}@r\text{GO}$ are shown in Fig. 4. Both rGO and $\text{PW}_{12}@r\text{GO}$ exhibit the type IV isotherm pattern with a H3 hysteresis loop, suggesting the mesoporous structures in these two materials. The BET surface area of the $\text{PW}_{12}@r\text{GO}$ composite is $103.48\text{ m}^2\text{ g}^{-1}$, which is significantly decreased compared to that of rGO ($849.17\text{ m}^2\text{ g}^{-1}$). In addition, the pore size distribution of $\text{PW}_{12}@r\text{GO}$ is also different from that of rGO (Fig. S4[†]). The decrease of the specific surface area and the change of the pore size distribution reveal that PW_{12} is successfully immobilized in the composite.

To confirm the elemental compositions and their oxidation states, XPS measurements were performed. As shown in Fig. 5a, characteristic peaks of W and P appear at 36.25 eV and 134.65 eV , respectively, indicating the successful immobilization of the PW_{12} catalyst. The C1s peaks could be deconvoluted with four contributions, corresponding to C–C (284.8 eV), C–O (286.3 eV), C=O (287.3 eV), and O–C=O (289.1 eV), respectively.³¹ The partial reduction of the starting material GO to reduced graphene oxide (rGO) during the hydrothermal process can be confirmed by the C1s high-resolution XPS spectra (Fig. 5b and c). It is obvious that the peak intensity of C–O in rGO is dramatically lower than that in GO (Fig. 5b–d). After immobilization of PW_{12} on the rGO support, the high-resolution XPS spectrum of C1s did not change, indicating that the introduction of POM did not change the structure of the support (Fig. 5d). In the XPS W4f spectrum of $\text{PW}_{12}@r\text{GO}$ (Fig. 5f), the peaks at binding energies of 36.0 eV (W $4f_{7/2}$) and

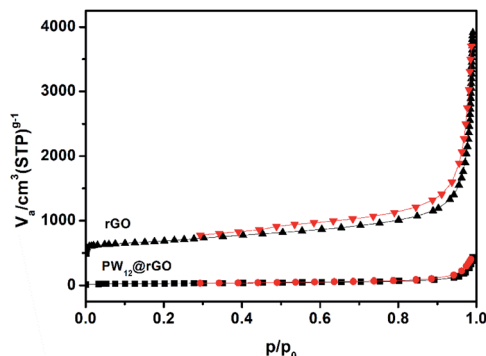


Fig. 4 The N_2 adsorption–desorption isotherms of rGO and $PW_{12}@rGO$.

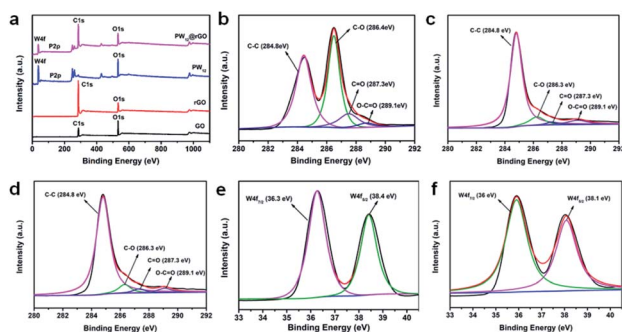


Fig. 5 XPS spectra: (a) survey spectra; C1s spectra of (b) GO, (c) rGO and (d) $PW_{12}@rGO$; XPS W4f spectra of (e) PW_{12} and (f) $PW_{12}@rGO$.

38.1 eV ($W 4f_{5/2}$) confirm the +6 oxidation state of W in the composite.⁴¹ Due to the strong electrostatic interaction between POM and the rGO support, electron density around W centers slightly increases, leading to a minor decrease of the W4f binding energy (0.3 eV) in $PW_{12}@rGO$ compared to that of the pristine PW_{12} cluster (Fig. 5e).

Epoxide ring-opening reactions catalyzed by the $PW_{12}@rGO$ monolith reactor

Epoxides are a type of versatile building block in organic synthesis, which can react with a variety of nucleophiles (such as alcohols, amines, and thiols) to obtain a broad range of commodity and fine chemicals.⁴² Ring-opening reactions between epoxides and alcohols is a useful route to produce β -alkoxy alcohols that are common organic solvents and important intermediates for the production of valuable chemicals.^{43,44} In general, this reaction can be accelerated by acidic and basic catalysts.⁴⁵ Until now, several kinds of heterogeneous catalysts have been developed for the epoxide ring-opening reaction.^{43,46} However, continuous flow reactors which can catalyze the epoxide ring-opening reaction under ambient conditions remains rarely reported.

In this work, the epoxide ring-opening reaction of styrene oxide with methanol was selected as a model reaction to evaluate the catalytic activity of $POM@rGO$ as a monolith reactor.

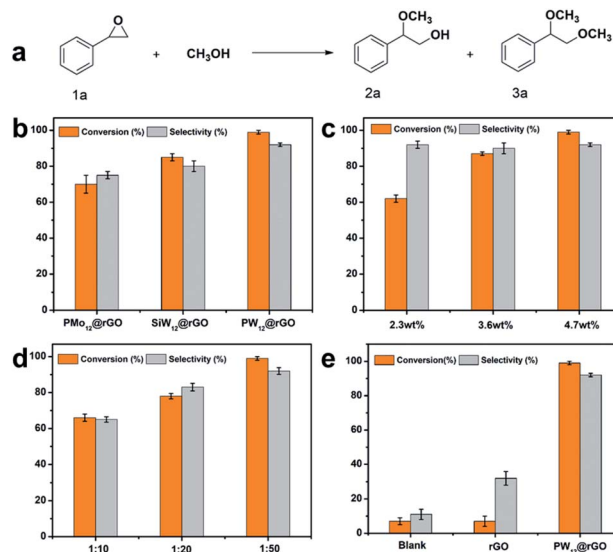


Fig. 6 (a) The epoxide ring-opening reaction of styrene oxide with methanol; (b) catalytic activity of three different $POM@rGO$ monolithic catalysts; (c) effect of PW_{12} loading amount on the conversion and selectivity of the epoxide ring-open reaction; (d) effect of the molar ratio of styrene oxide to methanol on the epoxide ring-open reaction; (e) the epoxide ring-opening reaction using different catalysts.

Generally, the ring-opening reaction of styrene oxide with methanol produces two products: **2a** and **3a** (Fig. 6a). For a typical reaction, styrene oxide (0.5 mmol) and biphenyl (internal standard, 0.3 mmol) were dissolved in methanol (1 mL) and then the reaction solution was absorbed by a block of $POM@rGO$ (diameter: 1 cm, height: 1 cm, mass: 20 mg, containing 0.00033 mmol PW_{12} species). As mentioned above, three different Keggin-type POM-modified rGO foams ($PMo_{12}@rGO$, $PW_{12}@rGO$ and $SiW_{12}@rGO$) have been successfully prepared and characterized (Fig. S5[†]). Experimental results show that all three $POM@rGO$ monolithic catalysts can catalyze the epoxide ring-opening reaction at room temperature without stirring (Fig. 6b). Among them, $PW_{12}@rGO$ exhibits the best performance, reaching a 99% conversion of the substrate in 10 min with a selectivity of 92% for product **2a**. It can be concluded that both the conversion and selectivity increase with the Brønsted acid strength of POMs, following an order of $PW_{12}@rGO > SiW_{12}@rGO > PMo_{12}@rGO$. Therefore, $PW_{12}@rGO$ was systematically investigated in the following epoxide ring-opening reactions.

To explore the optimal reaction conditions, the loading amount of the POM catalyst and the ratio of the substrate to methanol were systematically investigated. As shown in Fig. 6c, the conversion of styrene oxide significantly increases from 62% to 99% with the increase of PW_{12} loading with the selectivity for **2a** remaining basically unchanged. In this reaction, methanol acts as both solvent and reactant, and the catalytic activity of the ring-opening reaction shows a significant dependence on the ratio of styrene oxide to methanol. As shown in Fig. 6d, when the molar ratio of styrene oxide to methanol changes from 1 : 10, 1 : 20 to 1 : 50, the conversion of styrene oxide is

obviously increased from 66% to 99%, resulting in an improved selectivity for product **2a** accordingly.

To investigate the catalytic active center in $\text{PW}_{12}@r\text{GO}$, several control experiments were performed under the optimal reaction conditions. As shown in Fig. 6e, only 7% of styrene oxide was converted in the absence of the PW_{12} catalyst; simply using the rGO support as the catalyst led to a similar percentage of conversion but slightly improved selectivity. Using PW_{12} as a homogeneous catalyst can convert 94% of the substrate in 10 min with high selectivity for product **2a** (95%). Based on these results, we can conclude that the immobilized PW_{12} clusters are the dominant active centers in the monolith reactor, and the Brønsted acidity of $\text{PW}_{12}@r\text{GO}$ plays an important role during the reaction. To substantiate our conclusion, NH_3 -TPD measurements for $\text{PW}_{12}@r\text{GO}$ were performed. As shown in Fig. S6,† the absorption peaks at 128 °C and 282 °C correspond to weak acid sites and the mediate strong acid sites of $\text{PW}_{12}@r\text{GO}$, respectively. The total acidity capacity of $\text{PW}_{12}@r\text{GO}$ is calculated to be 2.1 mmol g^{-1} . The total acidic sites and the strength of the $\text{PW}_{12}@r\text{GO}$ composites were further characterized and quantified by the potentiometric titration method. Experimental results revealed that the immobilization of PW_{12} onto the rGO support could greatly enhance the Brønsted acidity of the composite (Fig. S7 and Table S1†). The initial electrode potential (E_i in mV) values of all three $\text{PW}_{12}@r\text{GO}$ composites with different PW_{12} loadings were calculated in the range of 499–566 mV (Fig. S7 and Table S1†) while the rGO support exhibits an E_i value of 59 mV, indicating the introduction of very strong acidic sites upon PW_{12} loading. Also, the number of acidic sites and the acidic strength increased accordingly with the increase of the amount of PW_{12} loading, which were consistent with the order of their catalytic activity towards the ring-opening reaction of styrene oxide with methanol (Fig. 6c). Therefore, the excellent catalytic performance of $\text{PW}_{12}@r\text{GO}$ might be attributed to the following two reasons: (1) POM clusters are highly dispersed on the support (Fig. 1b), thereby exposing more Brønsted acidic sites of $\text{PW}_{12}@r\text{GO}$ foam; (2) the lipophilic surface of the rGO support can greatly facilitate the contact of the hydrophobic organic substrate with hydrophilic POM centers.

To confirm the heterogeneity of the $\text{PW}_{12}@r\text{GO}$ reactor, the following experiments were performed. After the catalytic reaction, the catalytic reaction solution was separated, to which additional styrene oxide was added. At a similar reaction time, negligible conversion of styrene oxide was detected, that is comparable to that of the blank control test. The stable immobilization of POM on rGO foam was also checked by the leaching test. For a typical experiment, a block of the $\text{PW}_{12}@r\text{GO}$ monolith was soaked in methanol for 72 h and no characteristic absorption peak of PW_{12} in the solution was detected by UV-Vis spectroscopy (Fig. S8a†). Also, the FT-IR spectra of the reactor remained unchanged before and after immersion in methanol for 72 h (Fig. S8b†). These results further confirmed the stable immobilization of PW_{12} on rGO support.

In addition, the recyclability of the $\text{PW}_{12}@r\text{GO}$ monolith reactor was also evaluated. As shown in Fig. 7a, three blocks of similar $\text{PW}_{12}@r\text{GO}$ monolith reactors were placed in

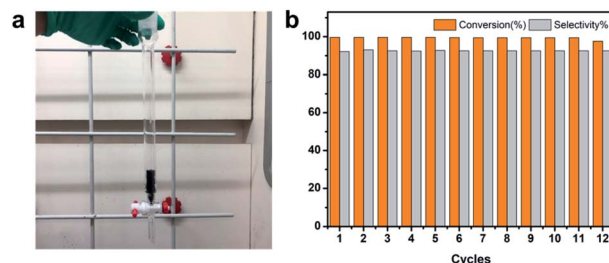


Fig. 7 (a) The digital image of the fixed bed batch reactor of $\text{PW}_{12}@r\text{GO}$ monolithic catalysts; (b) recycle test for the epoxide ring-opening reaction using $\text{PW}_{12}@r\text{GO}$ as the batch reactor. Reaction conditions: three blocks of the $\text{PW}_{12}@r\text{GO}$ monolithic catalyst (60 mg 4.7 wt% $\text{PW}_{12}@r\text{GO}$ composite, corresponding to 0.00099 mmol PW_{12} species), styrene oxide (1.5 mmol), methanol (3 mL), and biphenyl (internal standard, 0.9 mmol).

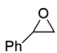
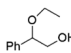
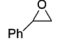
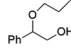
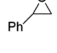
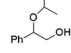
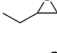
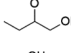
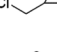
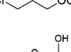
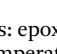
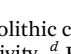
a chromatographic column, and the methanol solution of styrene oxide was slowly added. The reaction was performed under ambient conditions for 10 min, and then the reaction solution was pumped out to finish one catalytic cycle. After each cycle, the same amount of reaction solution was directly added to the column to start a new run. Impressively, the $\text{PW}_{12}@r\text{GO}$ monolith reactor can be readily reused without an obvious change of FT-IR spectra for at least twelve cycles without an obvious decrease of catalytic activity (Fig. 7b and S9†). Also, our $\text{PW}_{12}@r\text{GO}$ composite shows very high catalytic activity towards epoxide ring-opening of styrene compared to reported representative studies, and the TOF value is much higher than that of other heterogeneous catalysts (Table S2†). In addition, as a continuous flow monolith reactor, our catalytic system does not require mechanical stirring or heating during catalysis, which is very cost-effective and environmentally-benign.

Next, the scope of alcohols was also explored. Four different alcohols as nucleophiles were used to understand their influence on the ring-opening reaction (Table 1). The alcoholysis of styrene oxide with ethanol, n-propanol and i-propanol produces 2-ethoxy-2-phenylethanol, 2-propoxy-2-phenylethanol, and 2-isopropoxy-2-phenylethanol, respectively (Table 1, entries 1–3). With the increase of the carbon chain length, the reaction time to achieve similar conversion of the substrate increased from 10 min for methanol to 1.2 h for n-propanol. This phenomenon became more obvious when i-propanol with a branched chain was used; it took 2 h of reaction time to obtain 95% conversion of styrene oxide (Table 1, entry 3). These results reveal that the steric hindrance of the alcohol plays a significant role in the alcoholysis of styrene oxide. Then, we also evaluated the ring-opening reaction of three additional types of epoxides with methanol. It is found that such a $\text{PW}_{12}@r\text{GO}$ monolith reactor catalyzes more efficiently the methanolysis of the epoxide with an electron-donating group than that of the epoxide with an electron-withdrawing group (Table 1, entries 4–6).

Epoxide ring-opening reactions catalyzed by the $\text{PW}_{12}@r\text{GO}$ monolith flow reactor

The high catalytic performance and excellent recyclability of the $\text{PW}_{12}@r\text{GO}$ reactor prompted us to explore its potential

Table 1 Ring opening reaction of epoxide and alcohol by PW₁₂@rGO^a

| Entry | Epoxide | Alcohol | Product | Time (h) | Conv. ^b (%) | Sel. ^c (%) |
|-------|---|--------------------|---|----------|------------------------|-----------------------|
| 1 |  | Ethanol |  | 1 | 96 ^d | 90 |
| 2 |  | <i>n</i> -Propanol |  | 1.2 | 97 ^d | 93 |
| 3 |  | <i>i</i> -Propanol |  | 2 | 95 ^d | 91 |
| 4 |  | Methanol |  | 1 | 98 ^e | 45 |
| 5 |  | Methanol |  | 24 | 83 ^e | 100 |
| 6 |  | Methanol |  | 4 | 94 ^e | 51 |

^a Reaction conditions: epoxide (0.5 mmol), 4.7 wt% PW₁₂@rGO monolithic catalyst (20 mg, corresponding to 0.00033 mmol PW₁₂ species), alcohol (1 mL), and room temperature. ^b Conv. = conversion. ^c Sel. = selectivity. ^d Biphenyl as internal standard. ^e Naphthalene as internal standard.

application in continuous flow catalysis. The continuous flow set-up for the ring-opening reaction of styrene oxide with methanol is shown in Fig. 8a. The blocks of the PW₁₂@rGO (0.25 g) monolith was cut into small pieces and packed into a glass pipette as stated in the experimental part. Methanol solution containing styrene oxide and biphenyl (internal standard) was injected into the PW₁₂@rGO monolith flow reactor using a micro-injection pump at a flow rate of 0.1 mL min⁻¹. During the reaction, the amount of the reaction solution in the flow reactor remains constant and the product stream was collected using glass vials as 1 mL aliquots for further quantification by GC-FID. When the reaction solution flowed through the PW₁₂@rGO monolith flow reactor, the main product 2a was generated in very high yield. Remarkably, such a PW₁₂@rGO monolith flow reactor can continuously work at a high conversion level for 38 h with 99% conversion and over 90% selectivity, reaching a turnover number (TON) as high as 28 044 (Fig. 8b and S10†). More importantly, no obvious change can be observed in the IR spectra before and after the continuous flow catalysis (Fig. S11†), indicating the robustness and durability of the PW₁₂@rGO monolith flow reactor. It is noted that the catalytic activity of our continuous flow system slightly decreased with the prolonged reaction time after 38 h, which

could be attributed to the attachment of residual products onto the surface of the PW₁₂@rGO monolith reactor after several recycles. Since the rGO support is lipophilic, it is highly possible for the adsorption of product 2a onto the monolith reactor; such speculation has been confirmed by the presence of the FT-IR signal of product 2a after the catalytic reaction (Fig. S12†). Therefore, to maintain a good catalytic conversion yield and selectivity, it is better to run the reaction within 38 hours.

Conclusions

In summary, we reported a facile hydrothermal approach to construct POM@rGO foam as an effective monolith reactor to catalyze epoxide ring-opening reactions under mild conditions. The porous 3D structures of rGO foam exhibits a high surface area allowing the high dispersion of the POM catalyst onto the substrate through electrostatic interactions. The synthesized PW₁₂@rGO monolith reactor can effectively catalyze the epoxide ring-opening reaction of styrene oxide with methanol, achieving 99% conversion and 92% selectivity for the methanolysis product in 10 min under ambient conditions without stirring; such a PW₁₂@rGO monolith reactor can be readily reused for at least twelve cycles without an appreciable decrease of catalytic activity. More importantly, such a PW₁₂@rGO monolith flow reactor can continuously work at a high conversion level for 38 h with 99% conversion and over 90% selectivity, reaching a turnover number (TON) as high as 28 044. This present work not only provides a facile and broad-spectrum hydrothermal approach for the fabrication of a POM@rGO monolithic catalyst, but also offers new opportunities for the exploration of practical continuous flow apparatus for efficient catalysis in the future.

Author contributions

Xiaoting Jing: methodology, data curation, formal analysis, investigation, and writing—original draft preparation. Zhen Li: software. Weijie Geng: validation. Yingnan Chi: formal analysis,

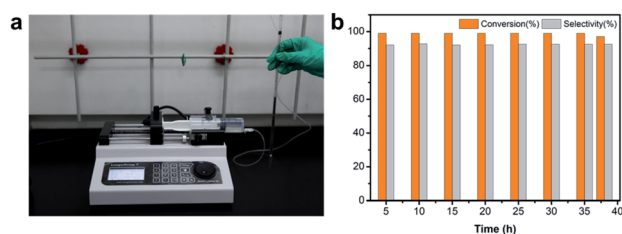


Fig. 8 (a) The digital image of a continuous flow set-up for the epoxide ring-opening reaction catalyzed by PW₁₂@rGO (0.25 g 4.7 wt%, corresponding to around 0.004 mmol PW₁₂ active species); (b) PW₁₂@rGO catalyzed epoxide ring-opening reaction in a continuous flow mode.

funding acquisition, project administration, conceptualization, supervision, and writing – reviewing and editing. Hongjin Lv: formal analysis, funding acquisition, project administration, supervision, and writing– reviewing and editing. Changwen Hu: funding acquisition, and supervision.

Conflicts of interest

There are no conflicts of interest to declare.

Acknowledgements

This work was supported by the National Natural Science Foundation of China (21671019, 21871025, 21871026, 21771020, and 21971010).

References

- 1 Y. Chen, X. Wu, L. Lv, F. Li, Z. Liu, Q. Kong and C. Li, *J. Colloid Interface Sci.*, 2017, **491**, 37–43.
- 2 Q. Jin, B. Lu, Y. Pan, X. Tao, C. Himmelhaver, Y. Shen, S. Gu, Y. Zeng and X. J. Li, *Catal. Today*, 2019, **327**, 279–287.
- 3 Q. Jin, Y. Shen, X. Li and Y. Zeng, *Mol. Catal.*, 2020, **480**, 110634.
- 4 C. T. Zhu, A. Gong, F. Zhang, Y. Xu, S. Sheng, F. A. Wu and J. Wang, *J. Chem. Technol. Biotechnol.*, 2019, **94**, 2569–2579.
- 5 Y. Liu, X. Liu, S. Yang, F. Li, C. Shen, C. Ma, M. Huang and W. Sand, *Nanomaterials*, 2018, **8**(9), 688.
- 6 Y. Liu, Y. Zheng, B. Du, R. R. Nasaruddin, T. Chen and J. Xie, *Ind. Eng. Chem. Res.*, 2017, **56**, 2999–3007.
- 7 N. Karbass, V. Sans, E. Garcia-Verdugo, M. I. Burguete and S. V. Luis, *Chem. Commun.*, 2006, **29**, 3095–3097.
- 8 Z.-C. Xiong, Z.-Y. Yang, Y.-J. Zhu, F.-F. Chen, R.-L. Yang and D.-D. Qin, *J. Mater. Chem. A*, 2018, **6**, 5762–5773.
- 9 C. H. Pelisson, T. Nakanishi, Y. Zhu, K. Morisato, T. Kamei, A. Maeno, H. Kaji, S. Muroyama, M. Tafu, K. Kanamori, T. Shimada and K. Nakanishi, *ACS Appl. Mater. Interfaces*, 2017, **9**, 406–412.
- 10 P. Ji, X. Feng, P. Oliveres, Z. Li, A. Murakami, C. Wang and W. Lin, *J. Am. Chem. Soc.*, 2019, **141**, 14878–14888.
- 11 S. Bolisetty, M. Arcari, J. Adamcik and R. Mezzenga, *Langmuir*, 2015, **31**, 13867–13873.
- 12 J. Zhou, C. Zhang and Y. Wang, *Polym. Chem.*, 2019, **10**, 1642–1649.
- 13 Y. Hou, D. Chai, B. Li, H. Pang, H. Ma, X. Wang and L. Tan, *ACS Appl. Mater. Interfaces*, 2019, **11**, 20845–20853.
- 14 M. Moghayed, E. K. Goharshadi, K. Ghazvini, H. Ahmadzadeh, R. Ludwig and M. Namayandeh-Jorabchi, *Mater. Chem. Phys.*, 2017, **188**, 58–67.
- 15 J. P. Tessonnier, S. Goubert-Renaudin, S. Alia, Y. Yan and M. A. Barteau, *Langmuir*, 2013, **29**, 393–402.
- 16 R. G. Prado, M. L. Bianchi, E. G. da Mota, S. S. Brum, J. H. Lopes and M. J. da Silva, *Waste Biomass Valorization*, 2017, **9**, 669–679.
- 17 M. Tao, N. Sun, Y. Li, T. Tong, M. Wielicako, S. Wang and X. Wang, *J. Mater. Chem. A*, 2017, **5**, 8325–8333.
- 18 J. Alcañiz-Monge, G. Trautwein and J. P. Marco-Lozar, *Appl. Catal., A*, 2013, **468**, 432–441.
- 19 W. Xie and F. Wan, *Chem. Eng. J.*, 2019, **365**, 40–50.
- 20 A. K. Dizaji, B. Mokhtarani and H. R. Mortaheb, *Fuel*, 2019, **236**, 717–729.
- 21 J. Alcañiz-Monge, B. E. Bakkali, G. Trautwein and S. Reinoso, *Appl. Catal., B*, 2018, **224**, 194–203.
- 22 A. I. Tropecêlo, M. H. Casimiro, I. M. Fonseca, A. M. Ramos, J. Vital and J. E. Castanheiro, *Appl. Catal., A*, 2010, **390**, 183–189.
- 23 A. E. R. S. Khder, H. M. A. Hassan and M. S. El-Shall, *Appl. Catal., A*, 2012, **411–412**, 77–86.
- 24 A. E. R. S. Khder, H. M. A. Hassan and M. S. El-Shall, *Appl. Catal., A*, 2014, **487**, 110–118.
- 25 R. Canioni, C. Roch-Marchal, F. Sécheresse, P. Horcajada, C. Serre, M. Hardi-Dan, G. Férey, J.-M. Grenèche, F. Lefebvre, J.-S. Chang, Y.-K. Hwang, O. Lebedev, S. Turner and G. Van Tendeloo, *J. Mater. Chem.*, 2011, **21**, 1226–1233.
- 26 F. Zhang, Y. Jin, J. Shi, Y. Zhong, W. Zhu and M. S. El-Shall, *Chem. Eng. J.*, 2015, **269**, 236–244.
- 27 Y. Wang, D. Shi, S. Tao, W. Song, H. Wang, X. Wang, G. Li, J. Qiu and M. Ji, *ACS Sustainable Chem. Eng.*, 2015, **4**, 1602–1610.
- 28 S. Doherty, J. G. Knight, M. A. Carroll, J. R. Ellison, S. J. Hobson, S. Stevens, C. Hardacre and P. Goodrich, *Green Chem.*, 2015, **17**, 1559–1571.
- 29 H. Zhang, Q. Zhang, L. Zhang, T. Pei, L. Dong, P. Zhou, C. Li and L. Xia, *Chem. Eng. J.*, 2018, **334**, 285–295.
- 30 X. Zhang, Y. Li, Y. Li, S. Wang and X. Wang, *ACS Appl. Nano Mater.*, 2019, **2**, 6971–6981.
- 31 R. Li, C. He, L. Cheng, G. Lin, G. Wang, D. Shi, R. K.-Y. Li and Y. Yang, *Composites, Part B*, 2017, **121**, 75–82.
- 32 T.-F. Li, X.-Q. Wang, J. Jiao, J.-Z. Liu, H.-X. Zhang, L.-L. Niu, C.-J. Zhao, C.-B. Gu, T. Efferth and Y.-J. Fu, *Renewable Energy*, 2018, **127**, 1017–1025.
- 33 W. Xie and M. Huang, *Energy Convers. Manage.*, 2018, **159**, 42–53.
- 34 L. Tan, D. Guo, J. Liu, X. Song, Q. Liu, R. Chen and J. Wang, *J. Electroanal. Chem.*, 2019, **836**, 112–117.
- 35 H. Hu, Z. Zhao, W. Wan, Y. Gogotsi and J. Qiu, *Adv. Mater.*, 2013, **25**, 2219–2223.
- 36 Y. Liu, S. Liu, X. Lai, J. Miao, D. He, N. Li, F. Luo, Z. Shi and S. Liu, *Adv. Funct. Mater.*, 2015, **25**, 4480–4485.
- 37 Y. Liu, F. Luo, S. Liu, S. Liu, X. Lai, X. Li, Y. Lu, Y. Li, C. Hu, Z. Shi and Z. Zheng, *Small*, 2017, **13**, 1603174.
- 38 X. Jing, Z. Li, B. Lu, Y. Han, Y. Chi and C. Hu, *Appl. Catal., A*, 2020, **598**, 117613.
- 39 Y. Xu, K. Sheng, C. Li and G. Shi, *ACS Nano*, 2010, **4**, 4324–4330.
- 40 M. Klein, A. Varvak, E. Segal, B. Markovskiy, I. N. Pulidindi, N. Perkas and A. Gedanken, *Green Chem.*, 2015, **17**, 2418–2425.
- 41 X. Kong, S. Wu, L. Liu, S. Li and J. Liu, *Mol. Catal.*, 2017, **439**, 180–185.
- 42 M. Mirza-Aghayan, M. Alizadeh, M. Molaee Tavana and R. Boukherroub, *Tetrahedron Lett.*, 2014, **55**, 6694–6697.

- 43 I. Matos, P. D. Neves, J. E. Castanheiro, E. Perez-Mayoral, R. Martin-Aranda, C. Duran-Valle, J. Vital, A. M. Botelho do Rego and I. M. Fonseca, *Appl. Catal., A*, 2012, **439–440**, 24–30.
- 44 C. J. Durán-Valle and J. A. García-Vidal, *Catal. Lett.*, 2009, **130**, 37–41.
- 45 H. Firouzabadi, N. Iranpoor, A. A. Jafari and S. Makarem, *J. Mol. Catal. A: Chem.*, 2006, **250**, 237–242.
- 46 D. Julião, A. D. S. Barbosa, A. F. Peixoto, C. Freire, B. de Castro, S. S. Balula and L. Cunha-Silva, *CrystEngComm*, 2017, **19**, 4219–4226.